Geochemical Perspectives Letters

Nitrogen isotope signatures of microfossils suggest aerobic metabolism 3.0 Gyr ago

F. Delarue, F. Robert, K. Sugitani, R. Tartèse, R. Duhamel, S. Derenne

Supplementary Information

The Supplementary Information includes:

- Studied Samples
- Sample Preparation, Microscopic Observation and Isotopic Analyses
- Biogenicity of the Studied Microfossils
- Reliability of the Morphological Traits and of the Geochemical Composition of Organic-walled Microfossils Isolated by Acid Maceration
- Assessing the Potential Effect of Contamination, Biomass Degradation and Fossilisation on $\delta^{15}N$ Values
- Biological Utilisation of NO_3^- and Anaerobic Ammonia Oxidation (Anammox)
- Tables S-1 and S-2
- Figures S-1 to S-6
- Supplementary Information References

Studied Samples

Three black chert samples were collected from the *ca*. 3.0 Ga Farrel Quartzite at the Mount Grant area in the Goldsworthy greenstone belt of the Pilbara Craton (Sugitani *et al*., 2007; Sugahara *et al*., 2010; Fig. S-1). This greenstone belt comprises a lower unit composed dominantly of volcanic sequences older than 3.17 Ga and the upper sedimentary succession of the 3.02–2.93 Ga De Grey Supergroup. The Farrel Quartzite, comprising the lower part of this sedimentary succession, is composed of a clastic formation up to 80 m thick, which contains fine- to very coarse-grained sandstone including quartzite with minor conglomerate, mafic to ultra-mafic volcanoclastic layers, evaporite beds and black chert layers. The *ca*. 30 cm thick fossil-bearing black chert occurs in the uppermost part of the Farrel Quartzite and is closely associated with evaporite beds (Fig. S-2). An association of black cherts and evaporites can be traced for *ca*. 7 km along strike in the central and the western parts of the greenstone belt. The Cleaverville Formation comprises the upper part of the 3.02–2.93 Ga De Grey Supergroup and is constituted by banded iron-formation, black shale, siltstone and chert in which one rock was sampled. Both Farrel Quartzite and Cleaverville cherts were metamorphosed in the greenschist facies corresponding for organic remnants to the carbonisation stage (Delarue *et al*., 2016). The fossil-bearing black chert have been deposited in shallow-evaporitic basin or shallow coastal sea since the chert bed (20 cm thick) is closely associated with evaporite beds, overlain by sandstone and bedded cherts. The abundance of sandstone decreases upward and the facies changes to more ferruginous horizons. The depositional environment likely changed from shallow-evaporitic basin to open ocean, which is consistent with rare earth element data (Sugahara *et al*., 2010).

Sample Preparation, Microscopic Observation and Isotopic Analyses

Kerogen acid isolation procedure from cherts

Bulk nitrogen isotopic composition ($\delta^{15}N_{Bulk}$, with respect to the $^{15}N/^{14}N$ ratio of the atmospheric N_2) was determined on 5 to 10 mg of organic matter (OM) previously isolated through successive demineralisation of *ca.* 200 g of rocks using hydrofluoric (HF) and hydrochloric (HCl) treatment (Derenne *et al.*, 2008). Powdered cherts were first stirred at room temperature in dichloromethane/methanol (2/1, v/v; High Performance Liquid Chromatography grade) in order to remove soluble organic compounds. Carbonates were then removed at room temperature using HCl (37 %; reagent grade) to minimise the formation of fluorides during maceration. Samples were then centrifuged and washed with distilled water until reaching neutrality. Concentration of organic matter was achieved through acid maceration at room temperature in a mixture of HF (40 %, reagent grade) and HCl (2/1, v/v; reagent grade). Samples were centrifuged and washed with distilled water to reach neutrality. Neoformed fluorides were then degraded using HCl (37 %; reagent grade) at 60 °C for 24 hours. After HCl hot acid maceration, kerogens were centrifuged and washed with distilled water until reaching neutrality.

Chemical and isotopic composition of bulk kerogen

Acid maceration residues were loaded in tin capsules and their N isotope composition (Table S-2) analysed using a CHN-elemental analyzer coupled to an isotopic ratio mass spectrometer (EA-IRMS; Flash 2000 - DeltaV Advantage). The analytical precision was determined within each run from analyses of alanine standards.

Sample mounting and microscopic observation

A few mg of isolated OM from one microfossil-bearing Farrel Quartzite black chert were dispersed in ethanol. This OM/ethanol mixture was either deposited on a glass slide as drops (NanoSIMS session 1) or filtered on a N-free polycarbonate filter (pore Ø = 10 μm; NanoSIMS session 2). After drying at room temperature, each preparation was directly coated with 20 nm gold. Before loading the sample in the vacuum chamber of the NanoSIMS, the microfossils were identified using transmission light microscopy directly on the glass slide and the polycarbonate filter. The different morphological features of the microfossils were ascribed following the taxonomy reported previously in both thin sections and acid-maceration residues (Sugitani *et al.*, 2007; Grey and Sugitani, 2009; Oehler *et al.*, 2009, 2010; House *et al.*, 2013). Three types of microfossil were identified: lenticular, spheroid and film-like microfossils. In the absence of unequivocal morphological features, the rest of the carbonaceous matter was assigned to the "amorphous carbonaceous matter" category. The analysed microfossils and amorphous carbonaceous matter particles were observed by Scanning Electron Microscopy (SEM) using a TESCAN VEGA II at the French National Museum of Natural History (MNHN), using an accelerating voltage of 15 kV (Fig. S-3).

NanoSIMS setup and calibration

The nitrogen isotopic composition of isolated microfossils ($\delta^{15}N_{\mu m}$) was analysed using the CAMECA NanoSIMS 50 at the NanoSIMS facility of the Muséum National d'Histoire Naturelle (MNHN) in Paris. The mass resolution was set to ≈10,000 (CAMECA definition) in order to resolve the isobaric interferences between the $^{12}C^{15}N^-$ on the one hand and $^{27}Al^-$, $^{26}MgH^-$, $^{11}B^{16}O^-$, $^{13}C^{14}N^-$ and $^{12}C_2H_3^-$ on the other hand. The high mass resolution scan around mass 27 displayed in Figure S-4 shows that the possible contribution of $^{13}C^{14}N^-$ molecular ions on the $^{12}C^{15}N^-$ measured at mass 27.040 (arrow on the Figure S-4) is negligible.

With a maximum contribution of ≤ 3 counts per second (cps) at 27.035 amu, the $\delta^{15}N$ variations measured at 27.040 amu (based on the measured $^{12}C^{15}N^-$ intensity) cannot be accounted for by a change in the carbon isotopic composition of the sample as reported by House *et al.* (2013). For example, a change in $\delta^{13}C$ of 20 ‰ corresponds to a relative variation of 2×10^{-4} on the $^{13}C^{14}N^-$ intensity and, therefore, to a corresponding shift in the $^{13}C^{14}N^-$ contribution from 3.0000 cps to 3.0006 cps. For a typical $^{12}C^{15}N^-$ signal around 200 cps, this would incur a negligible $\delta^{15}N$ shift of 3×10^{-3} ‰.

Before each measurement, the surface of target areas was presputtered with the primary Cs+ ion beam (440 pA with a 200 μm aperture diaphragm) until steady-state emission of the molecular ions $^{12}C^{14}N^-$ and $^{12}C^{15}N^-$ (Thomen, 2012). In order to reach a minimum value of 250 cps on the $^{12}C^{15}N^-$ signal, corresponding to a total of ca. 1×10^6 counts in about 1 hour of analysis and thus to a statistical Poisson error of ±1 ‰, the primary Cs+ beam current was adjusted in the two different sessions at ~12 pA and ~40 pA. Secondary $^{12}C^{14}N^-$ and $^{12}C^{15}N^-$ species were collected simultaneously by two electron multipliers. The data were corrected for a 44 ns dead time on each electron multiplier and were processed using the Limage software (developed by L. Nittler, Carnegie

Institution, Washington DC, USA).

Quasi-simultaneous arrivals (QSA) of secondary ions in electron multipliers can bias the determination of isotopic ratios (Slodzian *et al*., 2004). Figure S-5 shows the lack of correlation between the $^{12}C^{14}N^-$ secondary ion intensity (varying between 25,000 and 815,000 cps) and the instrumental mass fractionation (referred to as IMF and calculated from the measured $^{12}C^{15}N^-/^{12}C^{14}N^-$ ion ratio and the absolute $^{15}N/^{14}N$ ratio determined by standard mass spectrometric measurements for the type III standard kerogen). This range of $^{12}C^{14}N^-$ secondary ion intensity was obtained by using various co-axial lens diaphragms. In the case of the $\delta^{15}N_{\mu m}$ values reported here, most $^{12}C^{14}N^-$ secondary ion intensities range between ca. 50,000 and 250,000 cps (Table S-2) and, therefore, were not affected by any significant QSA effect. It is important to point out that the $1\sigma_{stat}$ error bars associated with each IMF determination presented in Figure S-5 were determined after 20-30 min analysis time on the type III kerogen standard, in contrast to the data reported in Tables S-1 and S-2 for Farrel Quartzite OM that correspond to analysis time of 60 minutes. This explains why the uncertainties displayed in Figure S-5 are much higher than those associated with data for Farrel Quartzite OM.

Two standards (coal for session 1 and type III kerogen for session 2) for which the absolute $^{15}N/^{14}N$ ratios have been determined using classical mass spectrometric analyses were analysed together with Farrel Quartzite OM in order to determine (i) the IMF and (ii) the reproducibility of $\delta^{15}N$ analysis (σ_{reprod}) during each analytical session (±2.3 ‰ and ±2.1 ‰ for the coal and type III kerogen, respectively; *cf*. Table S-1). The linearity of the mass spectrometer and the calibration setup of the NanoSIMS have been reported by Remusat *et al*. (2016). Note also that negative and positive $\delta^{15}N$ values were determined during the two distinct analytical sessions although the standard differed by 4.7 ‰ (from -1.0 ‰ for the coal to +3.7 for the kerogen III).

Surface microtopography and mineral matrix effects may cause analytical artifacts on the measured $^{12}C^{15}N^-/^{12}C^{14}N^-$ ionic ratio and, thus, on the determination of $\delta^{15}N_{\mu m}$ values. As shown by ion maps on individual microfossils, both microtopographic effects and mineral matrix effects (possibly caused by sub-micrometric mineral inclusions) do not bias the determination of the $^{12}C^{15}N^-/^{12}C^{14}N^-$ ionic ratio by more than ± 1.3 ‰, which corresponds to the standard error (1σ) obtained on the slope of the correlation $^{12}C^{15}N^-$ versus $^{12}C^{14}N^-$ (Fig. S-6).

For each individual microfossil, isotope ratios were determined at the bulk microfossil scale, *i.e*. for the whole sample surface but avoiding the sample edges.

The absolute $^{15}N/^{14}N$ ratios were calculated following:

$$(^{15}N/^{14}N)_{\mu m} = 1/IMF \times [^{12}C^{15}N^-]/[^{12}C^{14}N^-]$$

where the subscript "μm" indicates microfossil. IMF is the instrumental isotopic fractionation factor. The $^{15}N/^{14}N$ values are reported using the $\delta^{15}N_{AIR}$ (‰) notation, with $\delta^{15}N_{\mu m}$ (‰) = $\{[(^{15}N/^{14}N)_{\mu m} / (^{15}N/^{14}N)_{AIR}] - 1\} \times 1000$. All the $\delta^{15}N_{\mu m}$ values determined on microfossils and used in Figures 1 and 2 (in the main manuscript) are given in the Table S-2.

The statistical ion counting uncertainties (σ_{stat}) associated with the measured $^{12}C^{15}N^-/^{12}C^{14}N^-$ ionic ratios are approximated using the relationship:

$$\sigma_{stat} = [^{12}C^{15}N^-]^{-1/2} \qquad \text{Eq. S-1}$$

where $[^{12}C^{15}N^-]$ corresponds to the total number of counts (in most cases $[^{12}C^{15}N^-]$ was close to 10^6 counts, yielding σ_{stat} = 1‰).

The overall uncertainty (1σ) was calculated as:

$$1\sigma = \sqrt{\sigma_{stat}^{\ 2} + \sigma_{reprod}^{\ 2}} \qquad \text{Eq. S-2}$$

Biogenicity of the Studied Microfossils

The biogenicity of the Farrel Quartzite microfossils (lenses, spheres and films) has been demonstrated by a series of studies (Sugitani *et al*. 2007, 2009a, b; Sugahara *et al*., 2010; Oehler *et al*. 2009, 2010; Grey and Sugitani 2009; House *et al*. 2013; Delarue *et al*., 2017). Here we summarise the lines of evidence as follows:

1) The microstructures are contained in primary cherts without any evidence of metasomatic replacement (silicification) of precursory non-siliceous sediments. The matrix, in which the microfossils are embedded, is rich in cloudy carbonaceous particles, and locally forms lamination (Sugitani *et al*., 2007). Rare-earth elements and Y data suggest that the microfossil-bearing black cherts were precipitated from water masses of seawater compositions, with some input of continental run-off and/or low temperature hydrothermal fluids (Sugahara *et al*., 2010).

2) The microstructures are quite abundant. Their number in a normal petrographic thin section (2.8 × 4.7 cm in width and 30 µm in thickness) can be 100 or more. Colony-like clusters of lenses and spheres are common, and paired specimens as well (Sugitani *et al*., 2007).

3) The structures (small spheres and lenses) often comprise colony-like clusters. Paired and chained specimens are present. Size distributions of lenses and spheres are relatively narrow (Sugitani *et al*., 2007, 2009a).

4) The microstructures are composed of carbonaceous matter characterised by significantly light ($\delta^{13}C_{PDB}$ < -30‰) C isotopic values. Carbon isotopic values of lenses and spheres are distinct from the matrix carbonaceous particles (House *et al*., 2013). Nitrogen and sulphur are also detected in lenses and spheres (Delarue *et al*., 2017; Oehler *et al*., 2009, 2010)

5) The structures can be extracted by HF-HCl maceration, indicating that they are composed of acid-resistant membrane. This excludes the possibility that the structures were formed by redistribution of carbonaceous particles by crystal growths for example (Grey and Sugitani, 2009).

6) The microstructures display various taphonomic features, such as deformation and breakage. Wall textures vary from granular to hyaline, even within a single specimen (Sugitani *et al*., 2007, 2009b).

7) Many of the lenses are composed of a central spheroid body and surrounding sheet-like appendage called flange, which displays some variations of surface textures such as striation and reticulation (Sugitani *et al*., 2007, 2009b). Central bodies of most lenses, if not all, display intricate, internal network of organic materials (alveolar structure) (Oehler *et al*., 2010).

Reliability of the Morphological Traits and of the Geochemical Composition of Organic-walled Microfossils Isolated by Acid Maceration

Microfossils isolated by acid maceration from the Farrel Quartzite formation have been previously studied (*e.g*., Grey and Sugitani, 2009; Delarue *et al*., 2017). Acid maceration was also applied to other organic-walled microfossils from the 3.4 Gyr-old Strelley Pool Formation (Sugitani *et al*., 2015) and from the 3.3 Moodies Formation (Javaux *et al*., 2010).

From a morphological point of view, previous investigations suggest that acid maceration does not affect the integrity of Archean organic-walled microfossils (Javaux *et al*., 2010; Grey and Sugitani, 2009; Delarue *et al*., 2017).

From a geochemical point of view, preservation of N content was highly variable across individual microfossils isolated from the Farrel Quartzite (Delarue *et al*., 2017). This finding suggests that acid maceration does not lead to detectable N compounds hydrolysis since hydrolysis would have homogeneised N/C atomic ratios through the preferential degradation of chemically labile N moieties. This is consistent with the aromatic structures of Archean microfossils, making them more resistant to chemical degradation *via* hydrolysis compared to Proterozoic microfossils (as revealed by Raman microspectroscopy in numerous studies). In addition, isotopic fractionation *via* Rayleigh distillation cannot take place if the isotope exchange occurs between a solid (N in microfossils) and a fluid (N moieties in acid solution), indicating that the large $\delta^{15}N_{\mu m}$ variations cannot have resulted from such a process. Therefore, it is unlikely that acid maceration modified the N isotopic composition determined at the scale of individual microfossils by NanoSIMS.

Assessing the Potential Effect of Contamination, Biomass Degradation and Fossilisation on $\delta^{15}N$ Values

In organic matter, the $\delta^{15}N$ value reflects that of the dissolved inorganic nitrogen (DIN) pool(s) used by the source microorganisms, provided no contamination or nitrogen isotope fractionation was induced during biostratinomic and fossilisation processes.
First, contamination by N-compounds during the organic matter isolation procedure is unlikely since nitric acid and other N-bearing compounds are rigorously kept out during the acid maceration. In addition, contamination by exogenous N compounds cannot explain the large range of $\delta^{15}N\mu m$ values since modern OM is characterised by a narrow $\delta^{15}N$ range between ca. -6 to 0 ‰ (*e.g*., Thomazo *et al*., 2011). Extreme $\delta^{15}N$ variations are only found in some rare environments such as (i) the lake Kinneret or the Black sea (Coban-Yildiz *et al*., 2006; Hadas *et al*., 2009), which are characterised by large seasonal variations of the dominant nitrogen-metabolism, or (ii) in hydrothermal vents, in which the distance to the dissolved inorganic N source is the main controlling factor for its isotopic fractionation (Van Dover and Fry, 1994).

Biostratinomic process may also modify the original N isotopic composition of microorganisms. In modern marine

environments, NH_4^+ concentration gradient were observed within the upper levels of seafloor sediments (Boudreau and Canfield, 1988). In these sediments, NH_4^+ concentration gradient is related to biomass degradation occurring during biostratinomic processes. Biomass decay involves amino acid degradation which releases NH_4^+ that is readily available for assimilation. Nonetheless, according to Prokopenko *et al*. (2006), such a gradient is associated with restricted $\delta^{15}N$ variations of 3-4 ‰, consistent with incubation experiments (Lehmann *et al*., 2002). In addition, if NH_4^+ assimilation during biomass degradation in the host sediments was the main process responsible for the observed $\delta^{15}N_{\mu m}$ variations, there should not be any relationship between $\delta^{15}N_{\mu m}$ and microfossil types since all microfossils would have been randomly distributed in the metasediments. Therefore, the observed relationship between $\delta^{15}N_{\mu m}$ and microfossil types provides an additional criterion suggesting that significant N isotope fractionation did not occur during biostratinomic processes.

During fossilisation, temperature increase associated with burial can also potentially induce a shift of original N isotope compositions in response to thermal devolatilisation of ammonium (Bebout and Fogel, 1992). The Farrel Quartzite underwent metamorphism up to greenschist facies conditions (Sugitani *et al*., 2003; Sugitani *et al*. 2007; Delarue *et al*., 2016). During greenschist facies metamorphism, thermal devolatilization of ammonium can account for a limited $\delta^{15}N$ enrichment of *ca*. 1 to 2 ‰ (Bebout and Fogel, 1992; Boyd and Philippot, 1998; Ader *et al*., 2006). Moreover, all microfossil types display equivalent Raman line shapes, indicating that they all underwent a similar degree of thermal alteration (Sugitani *et al*., 2007). Thus, the wide range of $\delta^{15}N$ values observed for the microfossils does not depend on the degree of thermal alteration.

Finally, a large part of Archean metasedimentary rocks was post-depositionally silicified by pervasive secondary hydrothermalism (DeWit *et al*., 1982; Sugitani, 1992; Pinti *et al*., 2007). Hydrothermal alteration of metasediments can lead to $\delta^{15}N$ enrichment of up to ca. 10 ‰ (Pinti *et al*., 2009), which is not enough to account for the observed shift in $\delta^{15}N$ values by up to *ca*. 50 ‰. This is consistent with the fact that the Farrel Quartzite microfossil-bearing black cherts have not been intensively hydrothermally altered, as indicated notably by their weak or slightly positive europium anomaly that is absent in hydrothermal vein cherts (Sugahara *et al*., 2010).

As evidenced above, post-deposition processes such as contamination, thermal alteration and hydrothermalism cannot account for the whole range of $\delta^{15}N_{\mu m}$ variations observed at the microfossil scale. Therefore, the large $\delta^{15}N_{\mu m}$ variations measured in Farrel Quartzite microfossils likely reflect pristine N isotope signatures.

Biological Utilisation of NO_3^- and Anaerobic Ammonia Oxidation (Anammox)

The negative and positive $\delta^{15}N_{\mu m}$ values may reflect the uptake of distinct DIN sources, with $\delta^{15}N_{\mu m} < 0$ ‰ being attributed to the consumption of NH_4^+ through chemolithoautotrophy (Pinti *et al*., 2001; Pinti *et al*., 2009) while $\delta^{15}N_{\mu m} > 0$‰ would reflect the biological utilisation of NO_3^- (Sigman *et al*., 2009). However, the accumulation of NO_3^- in the water column and its subsequent utilisation by microorganisms would have required a rather high seawater redox state, which is *a priori* unlikely during mid-Archean times. During the mid-Archean, biological utilisation of NO_3^- is then unlikely. Such a conclusion is supported by phylogenomic studies (David and Alm, 2011).

Although our results support the early dominance of aerobic ammonium oxidizing microorganisms, the presence of anaerobic ammonium assimilating and oxidising (anammox) microorganisms remains an open issue. Indeed, opposite N isotope fractionations coexist in anammox metabolisms: formation of N_2 involves the uptake of ^{14}N from NH_4^+ and NO_2^- while the oxidation of NO_2^- into NO_3^- involves a preferential uptake of ^{15}N (Brunner *et al*., 2013). As far as we are aware, the resulting bulk $\delta^{15}N$ of the anammox biomass is unknown. Moreover, Archean waters are characterised by high dissolved ferrous iron concentrations (up to 120 µM; Canfield, 2005; Poulton and Canfield, 2011) and NO_2^- reduction by anammox in hydrothermal conditions may have been outcompeted by abiological reduction (Summers and Chang, 1993; Brandes *et al*., 1998). In addition, there is no consensus about the antiquity of anammox metabolism (Strous *et al*., 2006).

Supplementary Tables

Table S-1 NanoSIMS results obtained on the two OM standards used to determine the nitrogen isotope composition during the two analytical sessions ($\delta^{15}N_{bulk}$ of the coal and of the type III kerogen are -1.0 and +3.7 ‰, respectively). Ip corresponds to the intensity of the primary current and $^{12}C^{14}N^-$ and $^{12}C^{15}N^-$ correspond to the total ion counts (cts) of these respective species. $1\sigma_{stat}$ relates to the statistical ion counting uncertainty. The average IMF values (± reproducibility) are calculated for each analytical session.

		Ip (pA)	$^{12}C^{14}N^-$ (cts)	$^{12}C^{15}N^-$ (cts)	$1\sigma_{stat}$ (‰)	IMF
Session # 1	Coal_1	12	388287900	1455852	0.8	1.0246
Coal*	Coal_2	12	417846200	1561915	0.8	1.0215
	Coal_3	12	346461300	1292533	0.9	1.0195
	Coal_4	12	527888000	1978968	0.7	1.0245
	Coal_5	12	346461300	1292533	0.9	1.0195
	Coal_6	12	355228000	1325618	0.9	1.0198
Average Coal						**1.0216±0.0023**
Session # 2	Ker_III_1	40	430442300	1643454	0.8	1.0385
Type III kerogen*	Ker_III_2	40	442059100	1687416	0.8	1.0382
	Ker_III_3	40	287348000	1090387	1.0	1.0321
	Ker_III_4	40	107632800	409351	1.6	1.0344
	Ker_III_5	40	317557900	1210243	0.9	1.0366
	Ker_III_6	40	211493600	803351	1.1	1.0331
	Ker_III_7	40	116101800	441442	1.5	1.0342
	Ker_III_8	40	302033400	1152610	0.9	1.0380
	Ker_III_9	40	256275100	975270	1.0	1.0351
	Ker_III_10	40	280496700	1069260	1.0	1.0368
	Ker_III_11	40	244586600	932771	1.0	1.0373
	Ker_III_12	40	248707200	948307	1.0	1.0371
Average Type III kerogen						**1.0360±0.0021**

Table S-2 Nitrogen isotope compositions obtained on bulk kerogens (referred to as $\delta^{15}N_{Bulk}$; FQ: Farrel Quartzite; CF: Cleaverville Formation) using a CHN-elemental analyzer coupled to an isotopic ratio mass spectrometer (EA-IRMS) and on microfossils (A: Amorphous carbonaceous matter; F: Film-like microstructure; S: Spheroidal microstructure; L: Lenticular microstructure) using NanoSIMS (referred to as $\delta^{15}N_{\mu m}$). $^{12}C^{14}N^-$ and $^{12}C^{15}N^-$ correspond to the total ion counts (cts) of these respective species. $^{12}C^{14}N^-$ is also expressed in counts per second (cts s^{-1}). $^{15}N/^{14}N_{\mu m}$ corresponds to the $^{12}C^{15}N^-/^{12}C^{14}N^-$ ratio corrected for IMF, and $1\sigma_{stat}$ and 1σ relate to the statistical ion counting uncertainty and the total uncertainty (see Supplementary Information for details), respectively.

Session	$^{12}C^{14}N^-$ (cts)	$^{12}C^{15}N^-$ (cts)	$^{12}C^{14}N^-$ (cts s^{-1})	$^{15}N/^{14}N_{\mu m}$	$\delta^{15}N_{Bulk}$/ $\delta^{15}N_{\mu m}$	$1\sigma_{stat}$ (‰)	1σ (‰)	Rock sample/ Microfossil type
-	-	-			0.4	-	0.1	*FQ 1*
-	-	-			0.3	-	0.1	*FQ 2*
-	-	-			2.2	-	0.2	*CF*
#2	12756280	47362	25200	0.00358	-21.6	4.6	5.1	*A*
#2	44954960	169284	231131	0.00363	-7.7	2.4	3.2	*A*
#1	339316800	1260729	187297	0.00364	-7.4	0.9	2.5	*A*
#2	114356400	432773	166839	0.00365	-2.7	1.5	2.6	*A*
#2	110494600	417175	159287	0.00364	-5.1	1.5	2.6	*A*
#2	60497260	228554	61016	0.00365	-4.4	2.1	3.0	*A*
#2	132282200	501551	246538	0.00366	-0.8	1.4	2.5	*A*
#1	328959800	1231379	97278	0.00366	0.0	0.9	2.5	*A*
#2	253340000	944802	487939	0.00360	-17.2	1.0	2.3	*F*
#2	50445260	188405	159147	0.00361	-15.8	2.3	3.1	*F*
#2	23516410	88304	130502	0.00362	-10.5	3.4	4.0	*F*
#2	215178700	808886	162909	0.00363	-9.4	1.1	2.4	*F*
#2	70173560	263883	155845	0.00363	-9.0	1.9	2.9	*F*
#2	206757000	778486	154616	0.00363	-7.8	1.1	2.4	*F*
#2	79970460	302135	94294	0.00365	-4.4	1.8	2.8	*F*
#2	295731700	1119173	214392	0.00365	-2.7	0.9	2.3	*F*
#2	63871470	242753	244790	0.00367	1.6	2.0	2.9	*F*
#2	227089300	851314	176264	0.00362	-12.1	1.1	2.4	*S*
#2	180428200	677085	272386	0.00362	-11.1	1.2	2.4	*S*
#2	53982020	203321	176354	0.00364	-7.4	2.2	3.1	*S*
#2	207604100	782375	187886	0.00364	-6.9	1.1	2.4	*S*
#2	140804000	531690	135155	0.00365	-4.9	1.4	2.5	*S*
#2	26833340	101380	118001	0.00365	-4.4	3.1	3.8	*S*
#1	386553900	1447708	216565	0.00366	0.5	0.8	2.4	*L*
#1	347871100	1314596	68870	0.00370	9.5	0.9	2.5	*L*
#2	205515900	799004	234749	0.00375	24.5	1.1	2.4	*L*
#2	253920400	993119	191432	0.00378	30.7	1.0	2.3	*L*

Supplementary Figures

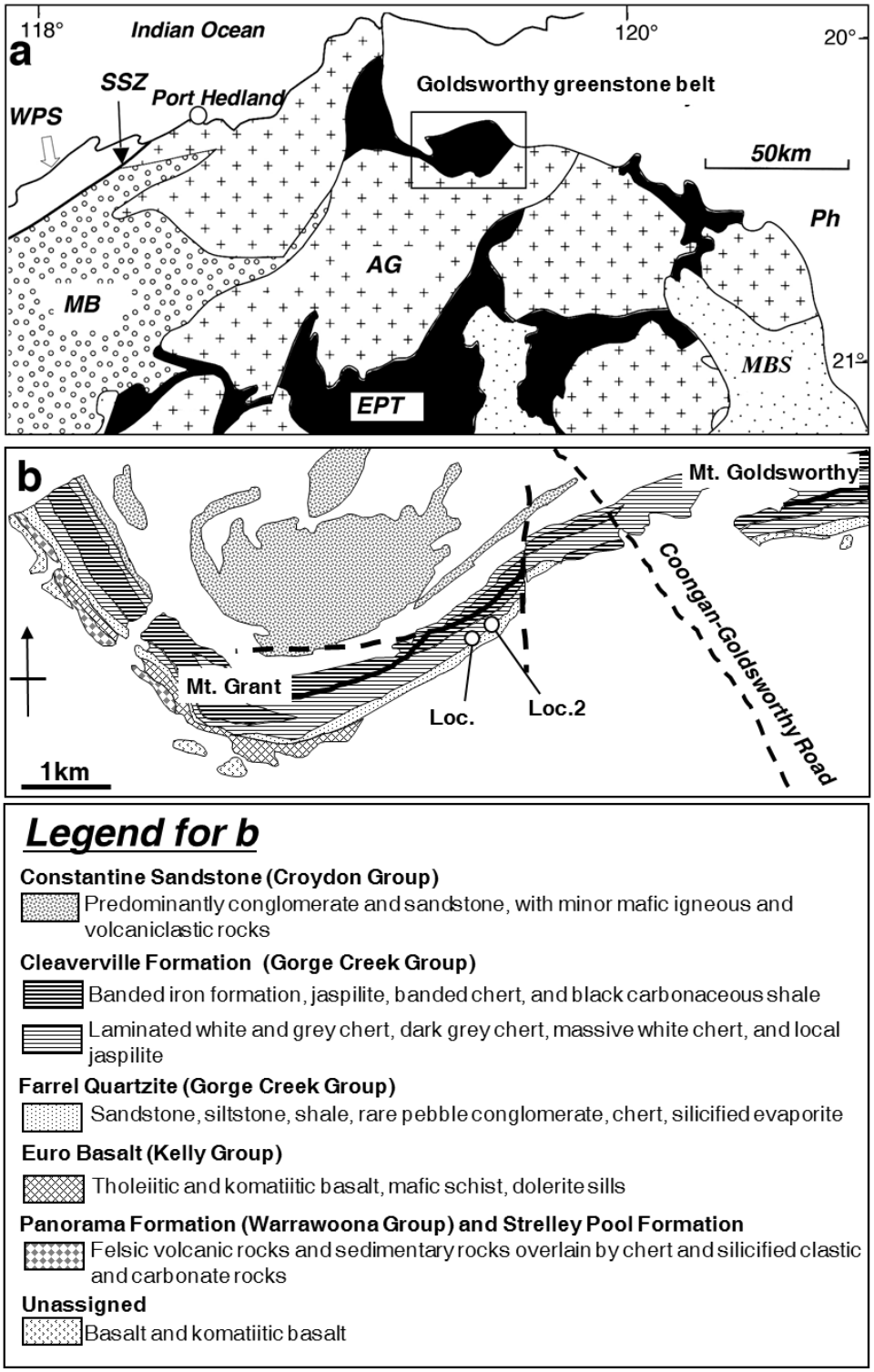

Figure S-1 **(a)** Geology of northeastern part of the Pilbara Craton. WPS: West Pilbara Superterrane, SSZ: Sholl Shear Zone, MB: Mallina Basin, AG: Archean granitic rocks, EPT: East Pilbara Terrane, MBS: Mount Bruce Supergroup, Ph: Phanerozoic cover. **(b)** Local geology of the Mount Goldsworthy – Mount Grant area, after Smithies *et al*. (2004) and Hickman (2008). Thick dashed line shows fault.

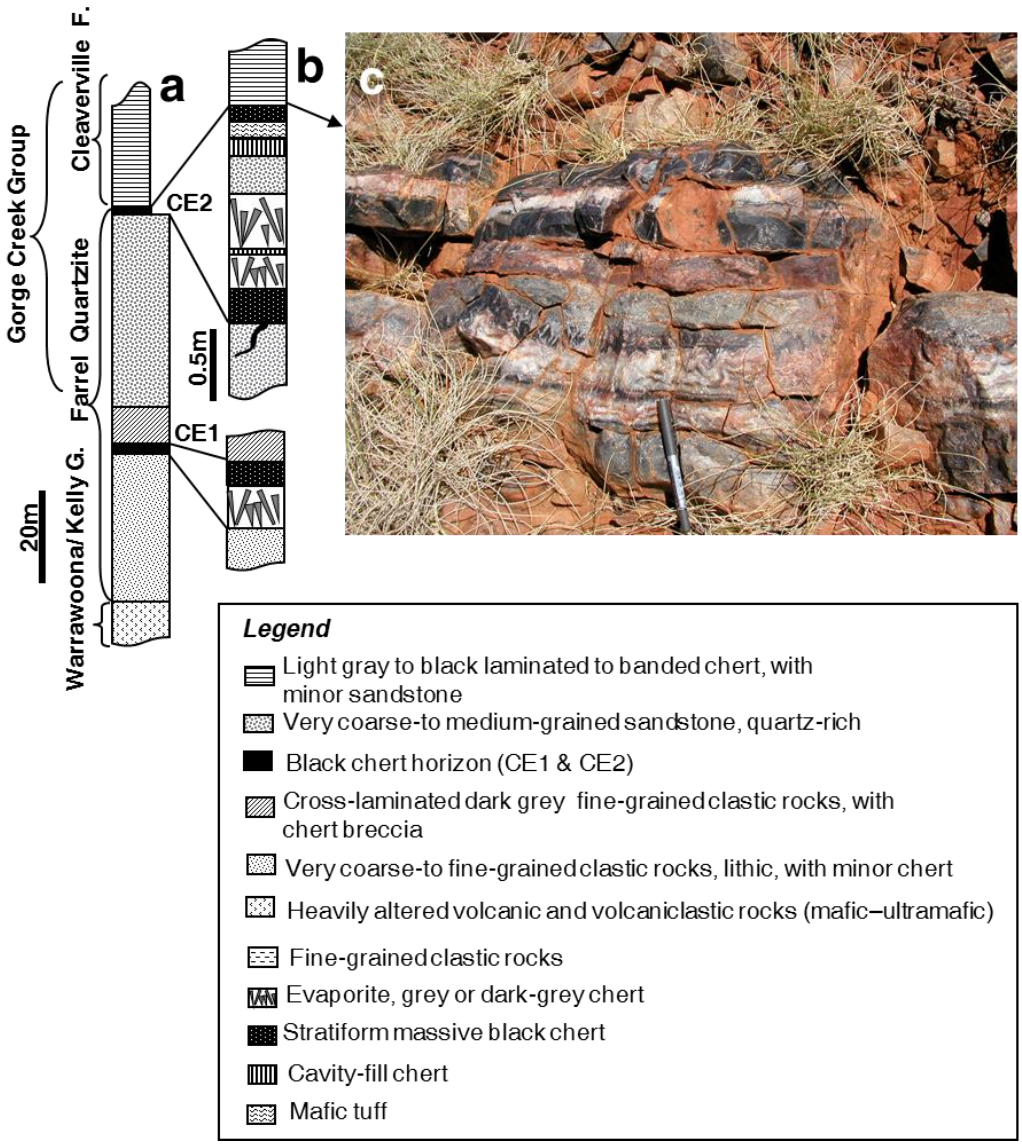

Figure S-2 **(a)** Stratigraphic column representing the section characterised by thick quartz-rich sandstone at Mount Grant, compiled from section data from Loc. 1 and Loc. 2 in Figure 1 (after Sugitani *et al.*, 2009b). **(b)** Details of horizons where black carbonaceous chert occurs in close association with evaporite beds. **(c)** Photograph of black chert containing microfossils inter-bedded with clastic bed and cavity-fill chert bed (top of the pen).

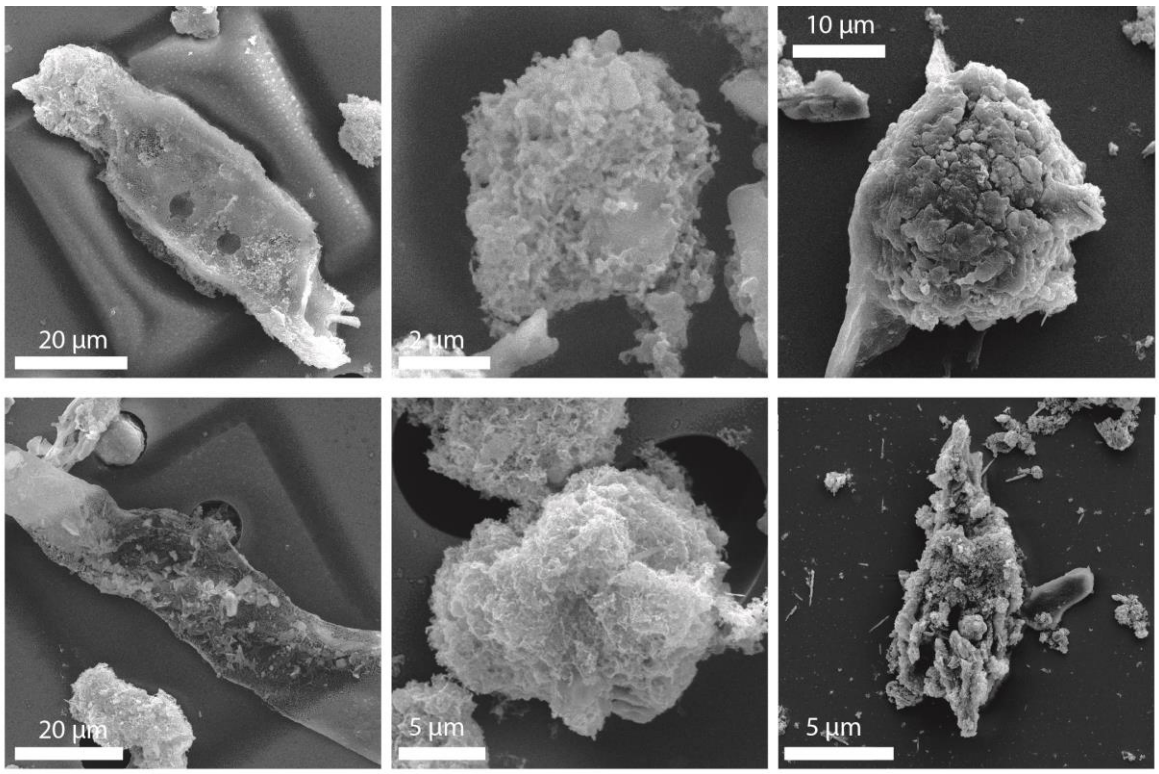

Figure S-3 SEM images of film-like (left column, spheroidal (middle column) and lenticular (right column) microfossils.

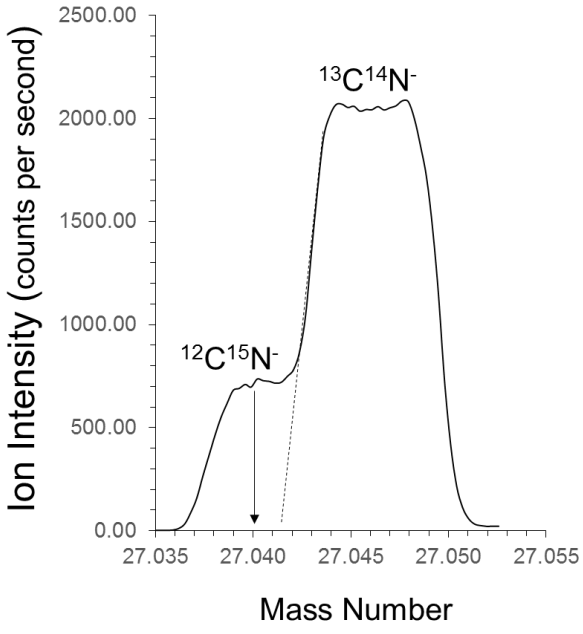

Figure S-4 High-resolution mass spectra for the mass region around 27 amu. The observed mass difference between the two peaks is consistent with the theoretical value of ~0.006 amu.

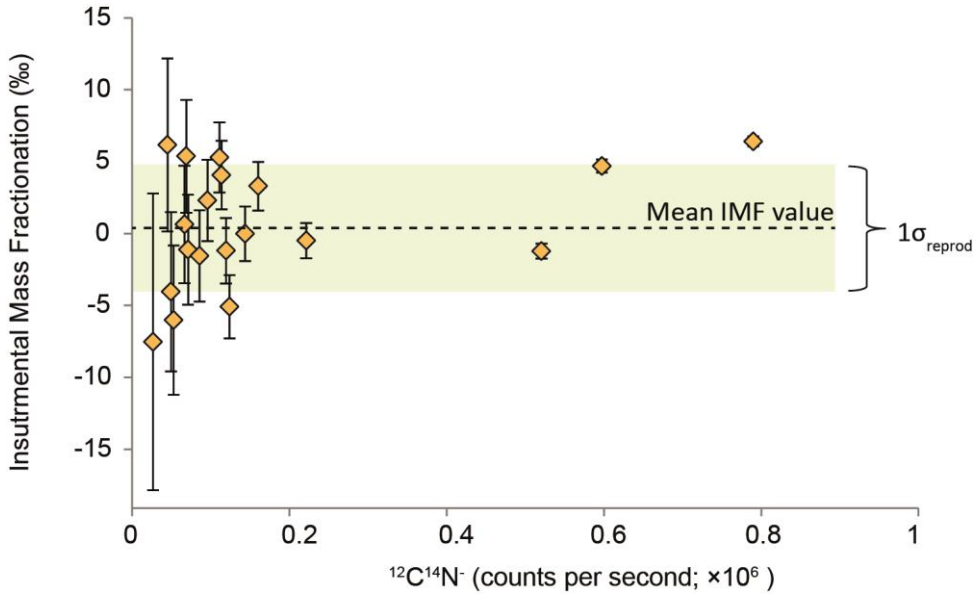

Figure S-5 Instrumental mass fractionation (IMF) expressed as a function of the $^{12}C^{14}N^-$ secondary ion intensity in counts per second ($\times 10^6$) determined on the type III kerogen standard. The green shaded area represents the $1\sigma_{reprod}$ and the dashed line corresponds to the mean IMF value. Except for one outlier corresponding to *ca*. 800,000 counts per second $^{12}C^{14}N^-$, all individual IMF values overlap (error bars correspond to $1\sigma_{stat}$) with the green area, showing that no QSA effect is detectable. The data reported in Table S-2 were obtained for $^{12}C^{14}N^-$ ranging between 2.5×10^4 and 2.7×10^5 cps, except for one film-like microfossil for which $^{12}C^{14}N^-$ was of *ca*. 4.9×10^5.

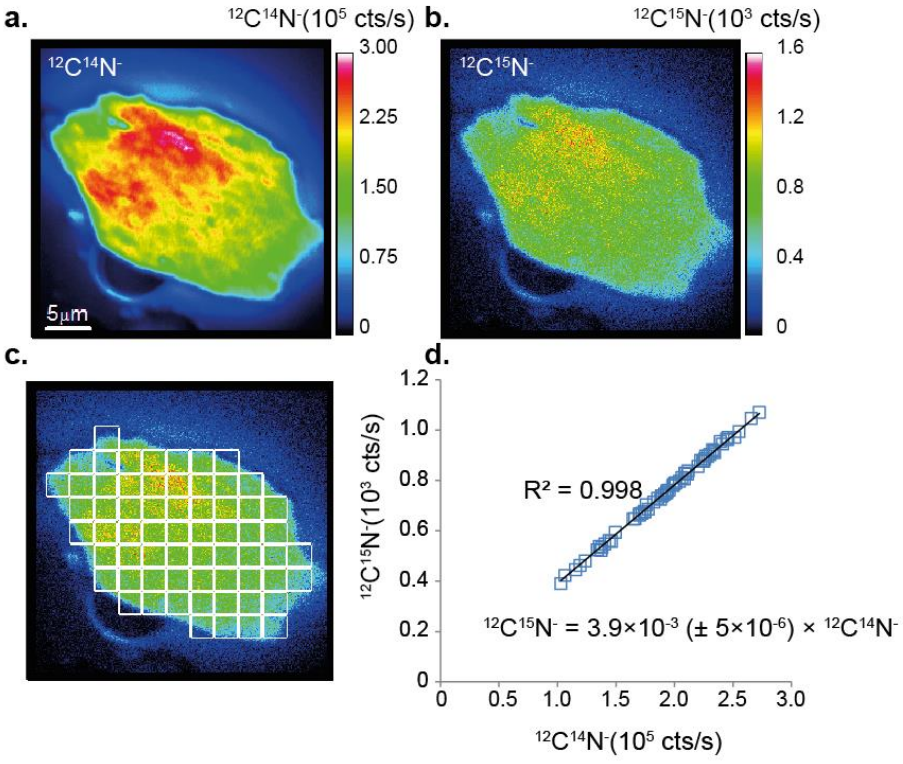

Figure S-6 **(a)** $^{12}C^{14}N^-$ map determined on a lenticular-like microfossil (see Fig. 1 in the main manuscript). **(b)** $^{12}C^{15}N^-$ map of the same lenticular-like microfossil (dark blue colors correspond to the polycarbonate filter; *cf*. text). **(c)** Selection of the regions of interest (ROI) reported in (d). **(d)** Relationship between the emissions of the $^{12}C^{14}N$- and $^{12}C^{15}N$- ionic species determined on each ROI.

Supplementary Information References

Ader, M., Cartigny, P., Boudou, J.P., Oh, J.H., Petit, E., Javoy, M. (2006) Nitrogen isotopic evolution of carbonaceous matter during metamorphism: Methodology and preliminary results. *Chemical Geology* 232, 152-169.

Bebout, G.E., Fogel, M.L. (1992) Nitrogen-isotope compositions of metasedimentary rocks in the Catalina schist, California - implications for metamorphic devolatilization history. *Geochimica et Cosmochimica Acta* 56, 2839-2849.

Boudreau, B.P., Canfield, D.E. (1988) A provisional diagenetic model for ph in anoxic porewaters - application to the foam site. *Journal of Marine Research* 46, 429-455.

Boyd, S.R., Philippot, P. (1998) Precambrian ammonium biogeochemistry: a study of the Moine metasediments, Scotland. *Chemical Geology* 144, 257-268.

Brandes, J.A., Boctor, N.Z., Cody, G.D., Cooper, B.A., Hazen, R.M., Yoder, H.S. (1998) Abiotic nitrogen reduction on the early Earth. *Nature* 395, 365-367.

Brunner, B., Contreras, S., Lehmann, M.F., Matantseva, O., Rollog, M., Kalvelage, T., Klockgether, G., Lavik, G., Jetten, M.S.M., Kartal, B., Kuypers, M.M.M. (2013) Nitrogen isotope effects induced by anammox bacteria. *Proceedings of the National Academy of Sciences of the United States of America* 110, 18994-18999.

Canfield, D.E. (2005) The early history of atmospheric oxygen: Homage to Robert A. Garrels. *Annual Review of Earth and Planetary Sciences* 33, 1-36.

Coban-Yildiz, Y., Altabet, M.A., Yilmaz, A., Tugrul, S. (2006) Carbon and nitrogen isotopic ratios of suspended particulate organic matter (SPOM) in the Black Sea water column. *Deep-Sea Research Part II-Topical Studies in Oceanography* 53, 1875-1892.

David, L.A., Alm, E.J. (2011) Rapid evolutionary innovation during an Archaean genetic expansion. *Nature* 469, 93-96.

Delarue, F., Robert, F., Sugitani, K., Tartese, R., Duhamel, R., Derenne, S. (2017) Investigation of the Geochemical Preservation of ca. 3.0 Ga Permineralized and Encapsulated Microfossils by Nanoscale Secondary Ion Mass Spectrometry. *Astrobiology* 17, 1192-1202.

Delarue, F., Rouzaud, J.N., Derenne, S., Bourbin, M., Westall, F., Kremer, B., Sugitani, K., Deldicque, D., Robert, F. (2016) The Raman-Derived Carbonization Continuum: A Tool to Select the Best Preserved Molecular Structures in Archean Kerogens. *Astrobiology* 16, 407-417.

Derenne, S., Robert, F., Skrzypczak-Bonduelle, A., Gourier, D., Binet, L., Rouzaud, J.-N. (2008) Molecular evidence for life in the 3.5 billion year old Warrawoona chert. *Earth and Planetary Science Letters* 272, 476-480.

Dewit, M.J., Hart, R., Martin, A., Abbott, P. (1982) Archean abiogenic and probable biogenic structures associated with mineralized hydrothermal vent systems and regional metasomatism, with implications for greenstone-belt studies. *Economic Geology* 77, 1783-1802.

Grey, K., Sugitani, K. (2009) Palynology of Archean microfossils (c. 3.0 Ga) from the Mount Grant area, Pilbara Craton, Western Australia: Further evidence of biogenicity. *Precambrian Research* 173, 60-69.

Hadas, O., Altabet, M.A., Agnihotri, R. (2009) Seasonally varying nitrogen isotope biogeochemistry of particulate organic matter in Lake Kinneret, Israel. *Limnology and Oceanography* 54, 75-85.

Hickman, A.H. (2008) Regional review of the 3426-3350 Ma Strelley Pool Formation, Pilbara Craton, Western Australia. *Geological Survey of Western Australia*, Record 2008/15.

House, C.H., Oehler, D.Z., Sugitani, K., Mimura, K. (2013) Carbon isotopic analyses of ca. 3.0 Ga microstructures imply planktonic autotrophs inhabited Earth's early oceans. *Geology* 41, 651-654.

Javaux, E.J., Marshall, C.P., Bekker, A. (2010) Organic-walled microfossils in 3.2-billion-year-old shallow-marine siliciclastic deposits. *Nature* 463, 934-939.

Lehmann, M.F., Bernasconi, S.M., Barbieri, A., McKenzie, J.A. (2002) Preservation of organic matter and alteration of its carbon and nitrogen isotope composition during simulated and in situ early sedimentary diagenesis. *Geochimica Et Cosmochimica Acta* 66, 3573-3584.

Oehler, D.Z., Robert, F., Walter, M.R., Sugitani, K., Allwood, A., Meibom, A., Mostefaoui, S., Selo, M., Thomen, A., Gibson, E.K. (2009) NanoSIMS: Insights to biogenicity and syngeneity of Archaean carbonaceous structures. *Precambrian Research* 173, 70-78.

Oehler, D.Z., Robert, F., Walter, M.R., Sugitani, K., Meibom, A., Mostefaoui, S., Gibson, E.K. (2010) Diversity in the Archean Biosphere: New Insights from NanoSIMS. *Astrobiology* 10, 413-424.

Pinti, D.L., Hashizume, K., Matsuda, J. (2001) Nitrogen and argon signatures in 3.8 to 2.8 Ga metasediments: Clues on the chemical state of the Archean ocean and the deep biosphere. *Geochimica et Cosmochimica Acta* 65, 2301-2315.

Pinti, D.L., Hashizume, K., Orberger, B., Gallien, J.P., Cloquet, C., Massault, M. (2007) Biogenic nitrogen and carbon in Fe-Mn-oxyhydroxides from an Archean chert, Marble Bar, Western Australia. *Geochemistry Geophysics Geosystems* 8.

Pinti, D.L., Hashizume, K., Sugihara, A., Massault, M., Philippot, P. (2009) Isotopic fractionation of nitrogen and carbon in Paleoarchean cherts from Pilbara craton, Western Australia: Origin of N-15-depleted nitrogen. *Geochimica et Cosmochimica Acta* 73, 3819-3848.

Poulton, S.W., Canfield, D.E. (2005) Development of a sequential extraction procedure for iron: implications for iron partitioning in continentally derived particulates. *Chemical Geology* 214, 209-221.

Prokopenko, M.G., Hammond, D.G., Spivack, A., Stott L. (2006) Impact of long-term diagenesis on δ15N of organic matter in marine sediments: sites. In Jorgensen, B.B., D'Hondt, S.L., Miller, D.J. (Eds.), Proceedings of the Ocean Drilling Program, Scientific Results 201, College Station, TX (Ocean Drilling Program).

Remusat, L., Piani, L., Bernard, S. (2016) Thermal recalcitrance of the organic D-rich component of ordinary chondrites. *Earth and Planetary Science Letters* 435, 36-44.

Sigman, D.M., Karsh, K.L., Casciotti, K.L. (2009) Nitrogen isotopes in the ocean.In: Steele J.H., Thorpe, S.A., Turekian, K.K. (Eds) *Encyclopedia of Ocean Sciences*, Academic Press, Oxford, 40–54.

Slodzian, G., Hillion, F., Stadermann, F.J., Zinner, E. (2004) QSA influences on isotopic ratio measurements. *Applied Surface Science* 231, 874-877.

Smithies, R.H. Van Kranendonk, M.J., Hickman, A.H. (2004) De Grey, W.A. Sheet 2757 (Version 2.0): *Western Australia Geological Survey*, 1:100 000 Geological Series.

Strous, M., Pelletier, E., Mangenot, S., Rattei, T., Lehner, A., Taylor, M.W., Horn, M., Daims, H., Bartol-Mavel, D., Wincker, P., Barbe, V., Fonknechten, N., Vallenet, D., Segurens, B., Schenowitz-Truong, C., Medigue, C., Collingro, A., Snel, B., Dutilh, B.E., Op den Camp, H.J.M., van der Drift, C., Cirpus, I., van de Pas-Schoonen, K.T., Harhangi, H.R., van Niftrik, L., Schmid, M., Keltjens, J., van de Vossenberg, J., Kartal, B., Meier, H., Frishman, D., Huynen, M.A., Mewes, H.W., Weissenbach, J., Jetten, M.S.M., Wagner, M., Le Paslier, D. (2006) Deciphering the evolution and metabolism of an anammox bacterium from a community genome. *Nature* 440, 790-794.

Sugahara, H., Sugitani, K., Mimura, K., Yamashita, F., Yamamoto, K. (2010) A systematic rare-earth elements and yttrium study of Archean cherts at the Mount Goldsworthy greenstone belt in the Pilbara Craton: Implications for the origin of microfossil-bearing black cherts. *Precambrian Research* 177, 73-87.

Sugitani, K. (1992) Geochemical characteristics of Archean cherts and other sedimentary-rocks in the Pilbara Block, Western Australia - evidence for Archean seawater enriched in hydrothermally-derived iron and silica. *Precambrian Research* 57, 21-47.

Sugitani, K., Mimura, K., Suzuki, K., Nagamine, K., Sugisaki, R. (2003) Stratigraphy and sedimentary petrology of an Archean volcanic-sedimentary succession at Mt. Goldsworthy in the Pilbara Block, Western Australia: implications of evaporite (nahcolite) and barite deposition. *Precambrian Research* 120, 55-79.

Sugitani, K., Grey, K., Allwood, A., Nagaoka, T., Mimura, K., Minami, M., Marshall, C.P., Van Kranendonk, M.J., Walter, M.R. (2007) Diverse microstructures from Archaean chert from the mount goldsworthy-mount grant area, pilbara craton, western australia: Microfossils, dubiofossils, or pseudofossils? *Precambrian Research* 158, 228-262.

Sugitani, K., Grey, K., Nagaoka, T., Mimura, K., Walter, M.R. (2009a) Taxonomy and biogenicity of Archaean spheroidal microfossils (ca. 3.0 Ga) from the Mount Goldsworthy-Mount Grant area in the northeastern Pilbara Craton, Western Australia. *Precambrian Research* 173, 50-59.

Sugitani, K., Grey, K., Nagaoka, T., Mimura, K. (2009b) Three-dimensional morphological and textural complexity of Archean putative microfossils from the Northeastern Pilbara Craton: Indications of biogenicity of large (>15μm) spheroidal and spindle-like structures. *Astrobiology* 9, 603-615.

Sugitani, K., Mimura, K., Takeuchi, M., Yamaguchi, T., Suzuki, K., Senda, R., Asahara, Y., Wallis, S., Van Kranendonk, M.J. (2015) A Paleoarchean coastal hydrothermal field inhabited by diverse microbial communities: the Strelley Pool Formation, Pilbara Craton, Western Australia. *Geobiology* 13, 522-545.

Summers, D.P., Chang, S. (1993) Prebiotic ammonia from reduction of nitrite by iron(ii) on the early Earth. *Nature* 365, 630-632.

Thomazo, C., Ader, M., Philippot, P. (2011) Extreme ^{15}N-enrichments in 2.72-Gyr-old sediments: evidence for a turning point in the nitrogen cycle. *Geobiology* 9, 107-120.

Thomen A. (2012) Développement instrumental de la mesure de l'hydrogène, du carbone et de l'azote à la NanoSIMS : applications à l'origine des volatils en cosmochimie. PhD thesis, French National Museum of Natural History.

Vandover, C.L., Fry, B. (1994) Microorganisms as food resources at deep-sea hydrothermal vents. *Limnology and Oceanography* 39, 51-57.